

A Technique for the Reduction of Banding in Landsat Thematic Mapper Images

Dennis L. Helder

Electrical Engineering Department, South Dakota State University, Brookings, SD 57007

Bruce K. Quirk

U. S. Geological Survey, EROS Data Center, Sioux Falls, SD 57198

Joy J. Hood

TGS Technology, Inc., EROS Data Center, Sioux Falls, SD 57198

ABSTRACT: The radiometric difference between forward and reverse scans in Landsat thematic mapper (TM) images, referred to as "banding," can create problems when enhancing the image for interpretation or when performing quantitative studies. Recent research has led to the development of a method that reduces the banding in Landsat TM data sets. It involves passing a one-dimensional spatial kernel over the data set. This kernel is developed from the statistics of the banding pattern and is based on the Wiener filter. It has been implemented on both a DOS-based microcomputer and several UNIX-based computer systems. The algorithm has successfully reduced the banding in several test data sets.

INTRODUCTION

BANDING, or differences between the forward and reverse scans of the Landsat thematic mapper (TM), has been a problem since the launch of Landsat-4 and has continued with Landsat-5. The TM instrument acquires data by using a scanning mirror system that collects data during both the forward and reverse scans. Both scans collect 16 lines of data for TM bands 1 through 5 and 7 and four lines of data for band 6. The problem is particularly evident over areas of very homogeneous response such as water, snow, or desert. It creates serious problems for researchers conducting quantitative studies over water bodies. The banding is normally most prominent in TM bands 1 through 4 and in TM-A data sets where it occurs every 16 lines, the number of lines in a forward or reverse scan.

Because banding is not entirely removed from these data sets during ground processing, this research addressed the development of a technique for alleviating banding in TM-P data sets. TM-A data sets are radiometrically corrected data sets, and TM-P data sets are radiometrically and geometrically corrected data sets.

The sources of TM banding have been identified by numerous studies associated with the evaluation of the radiometric and geometric properties of the Landsat TM sensor (Barker, 1985; Murphy *et al.*, 1985). Unfortunately, most of these studies dealt with A or pre-A data sets and not P data sets, the standard geometrically corrected product. Because A data have not been geometrically corrected, pixels generated by individual sensors can be identified and corrected for sensor gain and bias. Unfortunately, the resampling of A data to create P data causes this individual detector information to be lost. However, because researchers more frequently order geometrically corrected P data sets, this research focused on correcting banding in P data.

One source of radiometric variability is caused by a difference in offset between the forward and reverse scan calibrations. This effect is not correlated with the scene and may produce scan differences of up to four digital numbers (DN). Another source of banding is commonly termed "bright target overshoot" or "bright target saturation." This is caused when the detectors are scanned across a highly reflective target, such as clouds or snow cover, followed by a sharp transition to a region of lower reflectance. The detectors overshoot, which causes the scan to be darker than adjacent scans (Barker, 1985).

Malila and Metzler (1984) and Metzler and Malila (1985) noted that, due to scan-angle effects, the values at the western edge of the scene were higher than values at the eastern edge in TM data. They attributed these differences to nonsensor related effects such as atmospheric conditions. They also noted the difference in values between the forward and reverse scans. This was labeled "systematic droop" and occurred between the forward and reverse scans or approximately every 17 lines in P data. The droop was modeled as exhibiting an exponential decay and lasted for up to 1000 samples.

Kieffer *et al.* (1985) also noted the droop in bands 1 and 2 with a decay of approximately 1200 samples, in addition to the effects of scanning across bright targets. Desachy *et al.* (1985) noted both the bright target saturation effect and the radiometric hysteresis in their research with TM data. The effect was most dominant in bands 1 and 2, and the saturation caused by a snow field lasted up to 1000 pixels.

PREVIOUS EFFORTS TO REMOVE BANDING

Various methods of correcting for the radiometric inconsistencies in TM images have been proposed. These attempts can be divided into two categories: the first deals with correction of the A data and usually involves modifications to the individual detectors gain and bias or in generating a correction model, and the second category deals with the pattern as it exists in the P data. These techniques revolve around filtering to attenuate the banding.

Fusco *et al.* (1986) developed models to correct radiometric hysteresis, or overshoot/undershoot and droop, in Landsat TM data. They only applied their model to the bands of the first focal plane, bands 1 to 4, and used a decay time of approximately 10 ms or 1000 samples.

Murphy (1986) explained the radiometric correction procedures that are employed in the Canada Centre for Remote Sensing Landsat production system. These procedures are used to correct the effects of bright targets, such as snow or clouds, which caused up to a 4-DN shift and had a recovery time of up to 2000 pixels.

Engel *et al.* (1983) evaluated the radiometric performance of the TM sensor, noting the forward-reverse scan differences, and calculated fixed offsets to be applied to the first and last part of each forward scan.

Fischel (1984) found that using scan dependent biases would

reduce detector-to-detector, scan-to-scan, and multi-scan striping in TM images, but also noted the bright target saturation effect reported by other researchers. Recovery from the phenomenon was reported to take approximately 1000 pixels. Methods that involve gain and bias adjustments between forward and reverse scans assume that the user has geometrically uncorrected data (pre-P data) which is often not the case. Histogram modification methods also make this assumption (Poros and Peterson, 1985).

Because of the large size of the data sets (one Landsat TM scene requires approximately 250 MB of disk space), a computationally efficient algorithm is desirable. This means that transformation-based methods, such as principal components or fast Fourier transform approaches, may not be adequate. Transforming an image of this size into the frequency domain, performing some type of correction, and transforming the image back into the spatial domain is not feasible on most computer systems.

Because pixel values change not only between the forward and reverse scans but also along scans, the selected correction method must work on individual pixels and be based on local statistics. Methods that adjust entire lines of data are not as useful.

Srinivasan *et al.* (1988) proposed a spatial filtering method based on an average power spectrum. By averaging the spectra of vertical columns, those frequency components due to banding can be observed. By using smoothing and windowing operations, the peaks are isolated and then inverse Fourier transformed to produce a one-dimensional convolution kernel. Applying the kernel to an image reduced the banding pattern. Extending the same technique to two dimensions produced better results.

Another spatial filtering approach for TM-P data has been suggested by Crippen (1989). A three-pass operation was performed on the image that separated the banding pattern from the image data. The first pass was a 101-pixel averaging filter, horizontally oriented. Next, a filter using a vertical window averaged the data over 33 pixels. Subtracting this result from the first horizontal averaging step yielded a high-pass filter. For the third filtering operation, a low-pass filter was applied to the output of the second step. At this point, the banding was substantially isolated from the image and could be subtracted from the original.

Linear spatial filtering blurs edge information contained in an image (Gonzalez and Wintz, 1977) because edges contain energy at all frequencies. By removing some of these frequency components through a linear filtering operation, edges that were originally sharp become blurred. Both of the methods - Srinivasan and Crippen - discussed above are linear filters and therefore may blur edges. Crippen has noted this and suggests using thresholding, based on local statistics, to overcome this problem.

DEVELOPMENT OF A FILTER TO REMOVE BANDING

The development of a filter to correct banding is independent of the original cause of the banding. The banding occurs throughout the entire image, although it is most prominent in areas of low reflectance. The causes and effects of banding indicate that the correction method must depend on local statistics. To generate an appropriate filter, several observations of the banding phenomenon should be made:

- Banding noise is additive.
- Banding is predominantly vertically oriented and periodic.
- Banding noise variance is very small.

The first point allows modeling of the banding as a simple signal plus noise problem. It is assumed that no blurring of the image data has occurred. The second point allows approaching the

problem in one dimension. Although there are occasions when the noise pattern has a horizontal component, the algorithm developed can handle these situations with a simple modification. Therefore the observation at any point in the TM image may be described as

$$v(y) = s_{im}(y) + n(y) \quad (1)$$

where $v(y)$ is observed data; $s_{im}(y)$ is actual image data; $n(y)$ is banding noise; and the argument y indicates vertical position within a column of data or across the scan lines.

The third point expressed above indicates that banding is observed only at those image locations where the local image variance is also very small, which results in a low signal-to-noise ratio (SNR). Because the banding amplitude is less than 4 DN peak-to-peak, the corresponding variance is less than, or equal to, 4. As a result, banding is only observable over low variance, homogeneous regions. Therefore, the banding removal filter need only be applied to these areas; in other areas it is assumed that the SNR is large enough so that the noise component is negligible compared to the image data. Applying a filter in these regions may be counter productive in that some image detail may be removed along with the noise.

A one-dimensional linear filter, $h(y)$, is desired which minimizes the error between the observation and the true data value: i.e.,

$$\hat{s}_{im}(y) = h(y) * v(y) \quad (2)$$

where $\hat{s}_{im}(y)$ is an estimate of the correct data at location y and "*" denotes convolution. Choosing the minimum mean square error criterion results in the well-known Wiener filter with the corresponding covariance equation: i.e.,

$$K_{sv}(y) = h(y) * K_{vv}(y) \quad (3)$$

where $K_{vv}(y)$ is autocovariance of observation and $K_{sv}(y)$ is cross-covariance of the image and observation.

To form these covariance functions, it is assumed that the image data are independent of the noise. This assumption is reasonable if the banding pattern is caused by sensor miscalibration, but, when it is caused by bright target overshoot, there is an obvious correlation of the noise with the image. This problem can be resolved because the filter is only applied to those regions of the image where banding is objectionable and not across sharp transitions caused by bright targets. Thus, within the regions where the filter is applied, independence of data and noise is justified. Application of these ideas results in

$$K_{im}(y) = [K_{im}(y) + K_n(y)] * h(y) \quad (4)$$

where $K_{im}(y)$ is image autocovariance and $K_n(y)$ is banding autocovariance.

An expression for the banding autocovariance function can be developed by considering one column of data in which the banding pattern is prominent. Removing the image data and plotting the residual noise as a function of position would essentially yield a square-wave pattern. Positive peaks of the square-wave correspond to the alternating higher intensity scans, and negative peaks correspond to the lower intensity scans. The period of the square-wave is twice the width of a scan, usually about 34 pixels (because of resampling), and the amplitude (A), one-half of the peak-to-peak value, would then typically range from 0.5 to 2 DN. By assuming that the phase of this waveform is uniformly randomized over one period, the autocovariance for the banding becomes a triangular waveform with a period equal to twice the width of a scan. The positive peak is centered at the origin with a value equal to the square of the square-wave amplitude.

Many different image models could be used to generate the image autocovariance function. The key issue here is that the

model must describe an image region of very low variance where the banding occurs. One model that has performed satisfactorily in a number of applications represents the image as a first-order stationary Markov sequence (Jain, 1981). The autocovariance function for this model is

$$K_{im}(y) = \sigma_{im}^2 \tau^{|y|} \quad (5)$$

where σ_{im}^2 is image variance and τ is correlation coefficient ($0 < \tau < 1.0$). Image variance in regions where banding is prominent usually lies between 0 and 4. Typical values for τ that have yielded good results are $0.95 < \tau < 0.99$.

The expressions developed for the image and banding autocovariance functions can now be substituted into Equation 4, which is then solved for $h(y)$. The length of the filter window, although arbitrary, should follow some simple guidelines. Although the fundamental period of the banding is 32 pixels, it usually is somewhat larger because of the resampling process used in creating P data, usually 34 pixels. The minimum filter window should always cover an odd number of pixels so that the resulting filter can be zero-phase. From the symmetry present in the banding pattern, filter window sizes that are integer multiples of the banding period plus one pixel produce coefficient values that are all nearly zero. The exceptions are the coefficient located at the center of the filter window and those coefficients at distances from the center pixel that are integer multiples of the scan widths. In fact, the coefficients that are near zero in value are nonzero only because of the finite length of the filter window and computational accuracy. For example, a 35-weight filter has only three nonzero weights, one in the center and one at each end. The filter coefficients at the ends have the same value because of the symmetry present. Implementing this particularly sized filter involves only two adds and two multiplies at each pixel location where the filter is applied.

Table 1 shows values of filter coefficients for 35-weight filters as a function of correlation coefficient, τ , and SNR, $K_{im}(0)/K_n(0)$. Typically, SNR is less than unity in image regions where banding occurs. Equation 4 can be used to obtain filters that cover more than just three adjacent scans. Table 2 shows filter coefficient values for filters having lengths that are various multiples of the scan widths. In this table, $\tau = 0.99$ and $\text{SNR} = 0.25$, and the first column shows the values for a filter covering three

adjacent scans. Subsequent columns show filter coefficients that may be used for filters covering 5 to 11 scans. In both tables, the coefficient values have been normalized so that level shifting does not occur when the filters are applied; that is, the sum of all filter coefficients equals unity.

When the filter coefficients have been attained, a procedure must be developed to apply the filter only to image regions where the banding pattern is objectionable; that is, regions where the image variance is of the same order as, or smaller than, the banding variance. One approach is to apply a threshold to the difference in value between the center pixel in the filter window and pixels located at other nonzero coefficient positions. If the difference in value between the center pixel and a pixel located at a nonzero coefficient in the window is less than the threshold, that pixel is included in the calculations. If the difference is greater than the threshold, then that pixel is not included. As an example, consider a filter with a nonzero center coefficient and two nonzero coefficients displaced from the center by one scan width. At a given location in the image, if the difference in value between the center and both end pixels is less than the threshold, the filter is applied. If the difference is less than the threshold at one end and greater than the threshold at the other end, then the pixel at the end that exceeded the threshold is rejected and the pixel value at the other end is used in its place. If both ends yield differences that exceed the threshold, then the filter is not applied at that location and the center pixel value remains unchanged.

As with all thresholding operations, proper selection of the threshold is critical to success. Because the image variance has been modeled above and the banding amplitude is known to lie in a given range, one method to determine a proper threshold (T) is

$$T = 3\sigma_{im}^2 + 2A \quad (6)$$

Using typical values for the image variance and banding amplitude (A) gives $2.5 \leq T \leq 10$. For most images $3 \leq T \leq 5$.

IMPLEMENTATION AND RESULTS

The algorithm presented was initially prototyped by using a 286-based microcomputer equipped with a frame grabber card and transferred to a UNIX computer system under the Land Analysis System. The algorithm was implemented in the C programming language. Image size in all the examples shown is 512 by 512 pixels. Typical total elapsed times to process a three-band image of this size are from 2 to 3 minutes.

Plate 1 is a Landsat TM-P scene over the Prince William Sound area of Alaska. The image was obtained on 7 April 1989 (scene Y4245720350X0) as part of the study of the Valdez oil spill. This false-color composite (bands 4, 2, and 1) of quad 2 contains one of the study areas, which is outlined by a rectangle. The study area is a mixture of water and islands and the banding occurs every 16 to 17 lines in this data set. Figure 1 illustrates the "before" and "after" images for bands 1 to 4 and 6 of the study area. The banding pattern is clearly present in the water regions. A 35-weight filter was used with a center coefficient value of 0.5 and with a value of 0.25 at either end. Based on estimates of image variance and banding amplitude, a threshold was set at 5 by using Equation 6. The corresponding bands in the before and after figures have been identically stretched. Residual patterns in the after images are detector miscalibration or noise.

Figure 2 is a profile of an area containing only water pixels, the water area was averaged along scan to create a 512 by 1 pixel image for which a profile was generated. Both the before (Figures 2a to 2e) and after (Figures 2f to 2j) images were profiled. Note that the attenuation of the banding patterns in Figures 2a to 2e are at the same locations in Figures 2f to 2j and that the mean values remain the same, but the variance has

TABLE 1. FILTER COEFFICIENTS AS A FUNCTION OF SIGNAL-TO-NOISE RATIO (SNR) AND CORRELATION COEFFICIENTS (τ).

τ	SNR					
	0.1		1.0		10.0	
	middle	ends	middle	ends	middle	ends
0.90	0.50	0.25	0.58	0.21	0.84	0.08
0.95	0.50	0.25	0.56	0.22	0.80	0.10
0.99	0.50	0.25	0.52	0.24	0.64	0.18

TABLE 2. COEFFICIENT VALUES OF FILTERS OF VARIOUS LENGTHS WHERE τ IS 0.99 AND SNR IS 0.25.

Coefficient position (multiple of scan width)	Coefficient values				
	3 scans	5 scans	7 scans	9 scans	11 scans
0	0.50	0.77	0.83	0.89	0.83
1	0.25	0.25	0.16	0.12	0.16
2	—	-0.14	-0.16	-0.13	-0.16
3	—	—	0.09	0.13	0.09
4	—	—	—	-0.07	0.00
5	—	—	—	—	-0.002

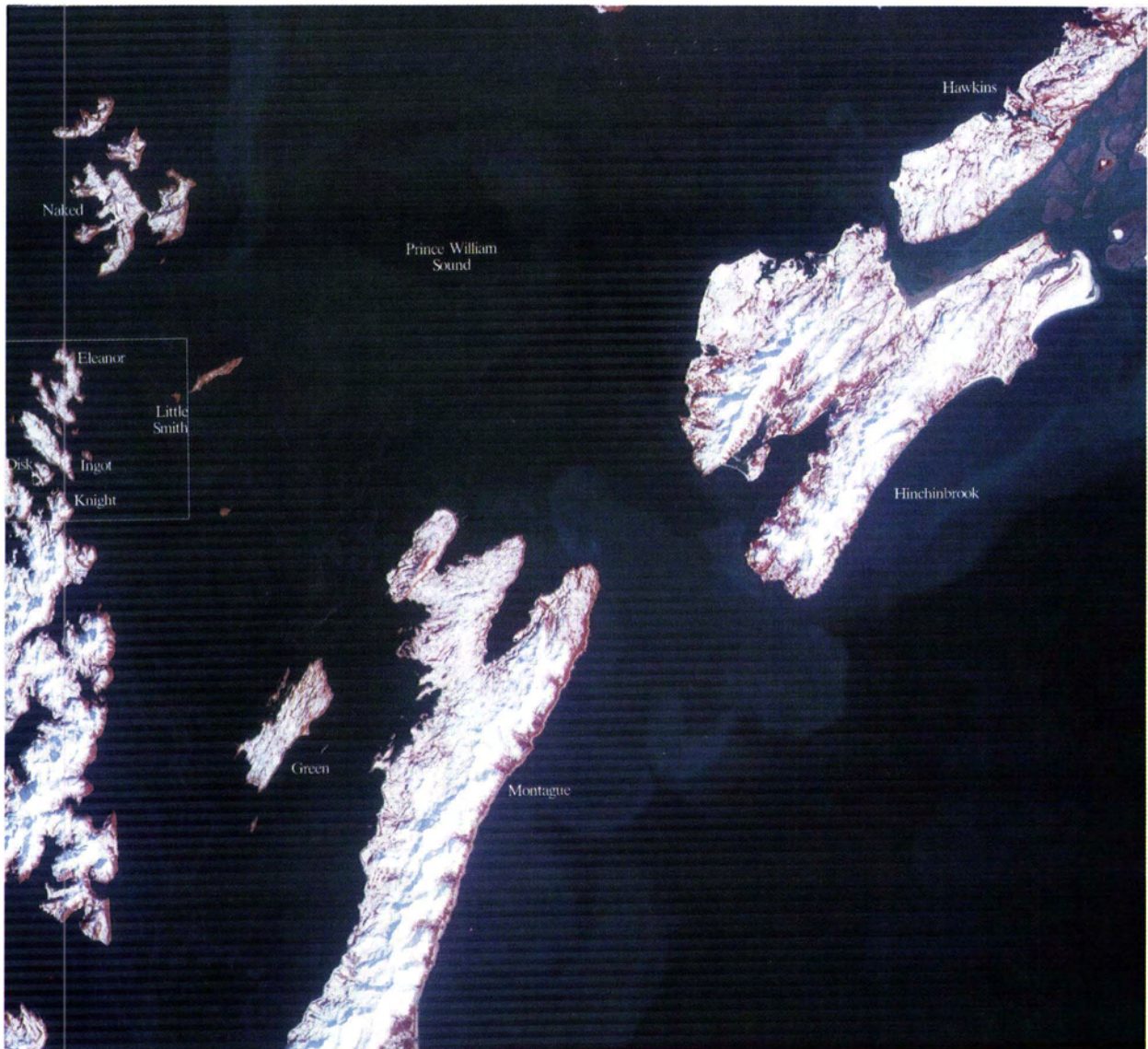


PLATE 1. Landsat thematic mapper P scene over Prince William Sound, Alaska. The image (scene Y4245720350X0) was obtained on 7 April 1989 and is a color composite of bands 4, 2, and 1 of quad 2.

been reduced in the filtered image. The means and standard deviations for the before and after profiles are presented in Table 3.

To validate the model, a column of data from the water region was extracted and the autocovariance function calculated. The result, shown in Figure 3a, clearly indicates the triangular waveform for the noise model. Here, the SNR is so low that the image autocovariance function cannot be viewed directly. Figure 3b shows the autocovariance for the same column of data after filtering. The triangular waveform due to the banding has been removed. The small peak remaining at a lag of 17 in Figure 3b indicates individual detector offset noise. This noise is caused by gain and bias differences between elements of the sensor array.

Two other study sites were also selected in the United Arab Emirates. The original Landsat scene, Y5130706134X0, was acquired on 29 September 1987. The first site, an area around Abu Dhabi, is shown in Plates 2a and 2b. Plate 2a shows the banding within the image, and Plate 2b shows the image after the tech-

TABLE 3. THE BEFORE AND AFTER MEAN AND STANDARD DEVIATIONS FOR A WATER AREA IN THE PRINCE WILLIAM SOUND STUDY AREA.

Band	Before		After	
	mean	standard deviation	mean	standard deviation
1	61.4	0.95	61.5	0.53
2	18.8	0.70	18.9	0.38
3	14.85	0.73	15.05	0.26
4	8.6	0.60	8.8	0.37
6	73.3	1.26	73.5	0.50

nique has been applied. A second site, a desert area, is shown in Plates 2c and 2d. Plate 2c shows the image before filtering, and Plate 2d shows the image after bands 3, 2, and 1 were filtered.

The filter operation is based on finding an average intensity value for three or more adjacent scans. Because the filter only

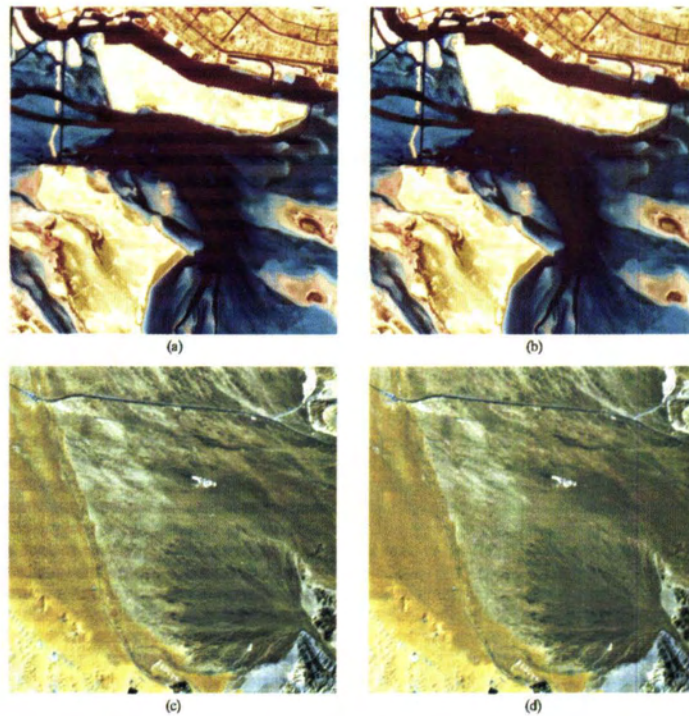


PLATE 2. Portions of Landsat thematic mapper image (scene Y5130706134X0) acquired on 29 September 1987 over the United Arab Emirates. The study areas are 512 lines by 512 samples. (a) Original bands 4, 3, and 2. (b) Filtered bands 4, 3, and 2. (c) Original bands 3, 2, and 1. (d) Filtered bands 3, 2, and 1.

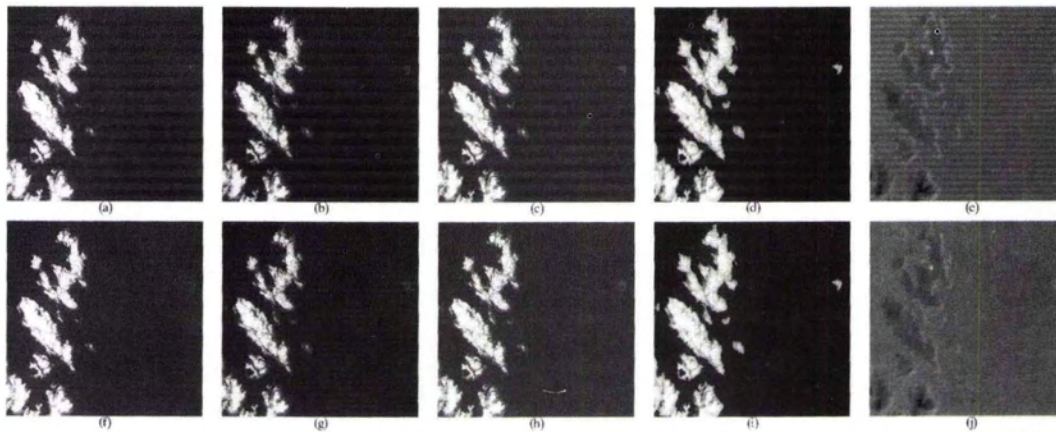


FIG. 1. Portion of Landsat thematic mapper image (scene Y4245720350X0) over Prince William Sound area of Alaska. Image area is 512 lines by 512 samples. (a) Original band 1. (b) Original band 2. (c) Original band 3. (d) Original band 4. (e) Original band 6. (f) Filtered band 1. (g) Filtered band 2. (h) Filtered band 3. (i) Filtered band 4. (j) Filtered band 6.

samples each scan at one location, an accurate reflection of the average intensity of that scan is not always obtained. Because of this, algorithm performance is better in low variance regions such as water than in desert regions. Although the algorithm retains edges with steps larger than the tolerance well, fine details that fall within tolerance limitations may generate artifacts in the filtered image. One approach that can be used to

reduce these effects is to use larger filter sizes covering several scans.

CONCLUSIONS

An algorithm was developed that significantly reduces the banding that is present in Landsat TM-P data. By modeling the noise pattern as a strictly one-dimensional square wave, a very

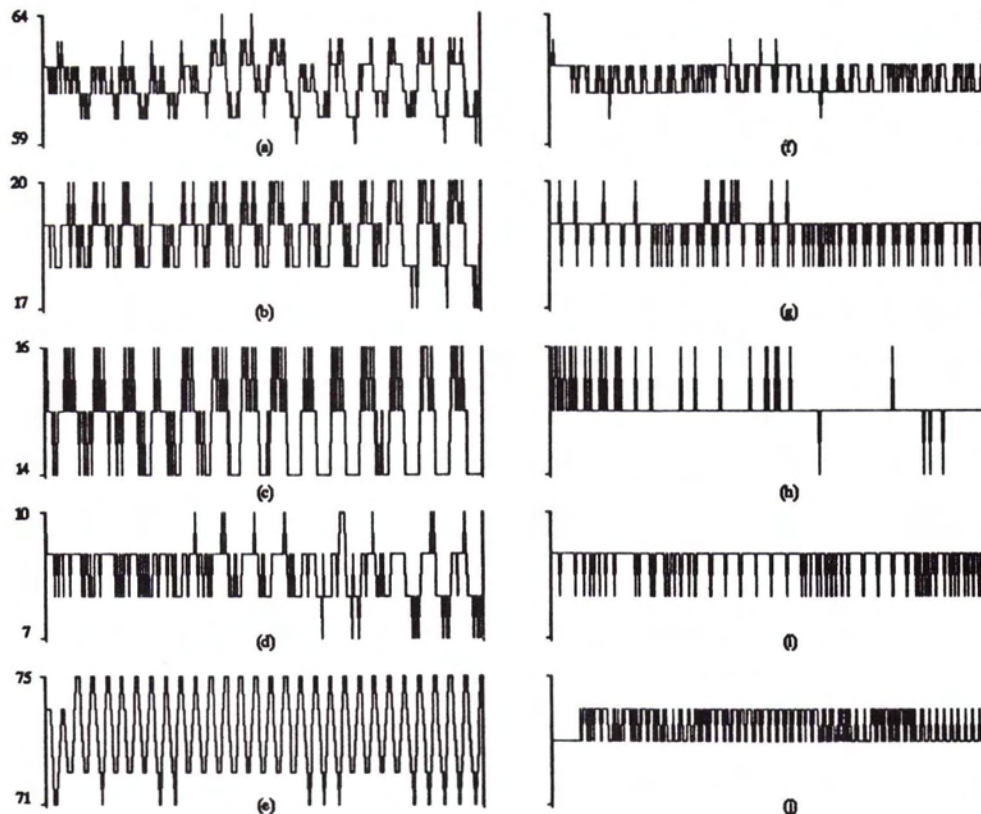


FIG. 2. Profiles of water pixels. The profiles represent an along scan average of a 500 line by 40 sample window extracted from the Prince William Sound study area. (a) Original band 1: mean = 61.4, standard deviation = 0.95. (b) Original band 2: mean = 18.8, standard deviation = 0.70. (c) Original band 3: mean = 14.85, standard deviation = 0.73. (d) Original band 4: mean = 8.6, standard deviation = 0.60. (e) Original band 6: mean = 73.3, standard deviation = 1.26. (f) Filtered band 1: mean = 61.5, standard deviation = 0.53. (g) Filtered band 2: mean = 18.9, standard deviation = 0.38. (h) Filtered band 3: mean = 15.05, standard deviation = 0.26. (i) Filtered band 4: mean = 8.8, standard deviation = 0.37. (j) Filtered band 6: mean = 73.5, standard deviation = 0.50.

efficient spatial filter implementation can be developed by using the minimum mean square error criterion. Because the noise variance is very low, typically less than 4 DN, the filter only needs to be applied where image variance is of the same order such that the resulting SNR is small. These areas are identified by applying a threshold to differences between the value of the pixel being filtered and the values of the pixels within the filter window that are associated with nonzero coefficients. The radiometric quality of both the Alaska and United Arab Emirates scenes were improved with the use of the filter.

Efforts to improve the algorithm, and overcome the limitations described above, are being directed toward investigating the advantages of a two-dimensional filter structure, more accurate modeling of the banding pattern to take into account the resampling to P-data, and removal of any scene dependencies from the filter parameters.

ACKNOWLEDGMENTS

Worked performed under U.S. Geological Survey contract 14-08-0001-22521. Any use of trade, product, or firm names in this publication is for descriptive purposes only and does not imply endorsement by the U.S. Government.

REFERENCES

Barker, J. L., 1985. Relative radiometric calibration of Landsat TM reflective bands, *Proceedings of the Landsat-4 Science Characterization*

Early Results Symposium, Greenbelt, Maryland, 22-24 February 1983, NASA Conference Publication 2355, Vol. 3, pp. 1-219.

Crippen, R. E., 1989. A simple spatial filtering routine for the cosmetic removal of scan-line noise from Landsat TM P-tape imagery, *Photogrammetric Engineering & Remote Sensing*, Vol. 55, No. 3, pp. 327-331.

Desachy, J., G. Begni, B. Boissin, and J. Perbos, 1985. Investigation of Landsat-4 thematic mapper line-to-line and band-to-band registration and relative detector calibration, *Photogrammetric Engineering & Remote Sensing*, Vol. 51, No. 9, pp. 1291-1298.

Engel, J. L., J. C. Lansing, D. G. Brandshaft, and B. J. Marks, 1983. Radiometric performance of the thematic mapper, *Proceedings of the Seventeenth International Symposium on Remote Sensing of Environment*, Ann Arbor, Michigan, 9-13 May, Vol. 1, pp. 293-317.

Fischel, D., 1984. Validation of the Thematic Mapper radiometric and geometric correction algorithms, *IEEE Transactions on Geoscience and Remote Sensing*, Vol. GE-22, No. 3, pp. 237-242.

Fusco, L., U. Frei, D. Trevese, P. N. Blonda, G. Pasquariello, and G. Milillo, 1986. Landsat TM image forward/reverse scan banding: characterization and correction, *International Journal of Remote Sensing*, Vol. 7, No. 4, pp. 557-575.

Gonzalez, R. C., and P. Wintz, 1977. *Digital Image Processing*, Addison-Wesley Publishing Company, Reading, Pennsylvania, 431 p.

Jain, A. K., 1981. Advances in Mathematical Models for Image Processing, *IEEE Proceedings*, Vol. 69, No. 5, pp. 502-528.

Kieffer, H. H., D. A. Cook, E. M. Eliason, and P. T. Eliason, 1985. Intraband radiometric performance of the Landsat Thematic Mappers, *Photogrammetric Engineering & Remote Sensing*, Vol. 51, No. 9, pp. 1331-1350.

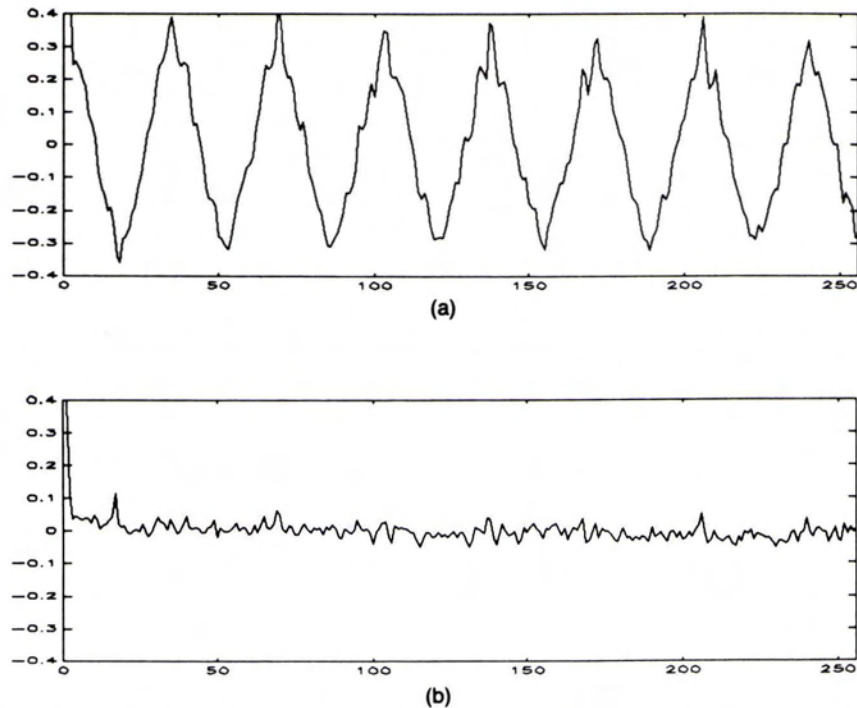


FIG. 3. Autocovariance for band 3 of the Alaskan scene before filtering (a). Autocovariance for band 3 of the Alaskan scene after filtering (b).

- Malila, W. A., and M. D. Metzler, 1984. Characterization of Landsat-4 MSS and TM digital image data, *IEEE Transactions on Geoscience and Remote Sensing*, Vol. GE-22, No. 3, pp. 177-191.
- Metzler, M. D., and W. A. Malila, 1985. Characterization and comparison of Landsat-4 and Landsat-5 Thematic Mapper data, *Photogrammetric Engineering & Remote Sensing*, Vol. 51, No. 9, pp. 1315-1330.
- Murphy, J. M., 1986. Within-scene radiometric correction of LANDSAT Thematic Mapper (TM) data in Canadian production systems, *Proceedings of the Earth Remote Sensing Using Landsat Thematic Mapper and SPOT Sensor Systems*, Innsbruck, Austria, 15-17 April, SPIE, Vol. 660, pp. 25-31.
- Murphy, J. M., F. J. Ahern, P. F. Duff, and A. J. Fitzgerald, 1985. Assessment of radiometric accuracy of Landsat-4 and Landsat-5 Thematic Mapper data products from Canadian production systems, *Photogrammetric Engineering & Remote Sensing*, Vol. 51, No. 9, pp. 1359-1369.
- Poros, D. J., and C. J. Peterson, 1985. Methods for destriping Landsat Thematic Mapper images-A feasibility study for an online destriping process in the Thematic Mapper Image Processing System (TIPS), *Photogrammetric Engineering & Remote Sensing*, Vol. 51, No. 9, pp. 1371-1378.
- Srinivasan, R., M. Cannon, and J. White, 1988. Landsat data destriping using power spectral filtering, *Optical Engineering*, Vol. 27, No. 11, pp. 939-943.

OFFICIAL NOTICE TO ALL CERTIFIED PHOTOGRAMMETRISTS

The ASPRS Board of Directors approved an expansion of the Certified Photogrammetrist Program that goes into effect **January 1, 1992**. After that date, all Certified Photogrammetrists **MUST** submit an application for recertification as a Photogrammetrist or for certification as a "Certified Mapping Scientist--Remote Sensing," or "Certified Mapping Scientist--GIS/LIS." Recertification is required every five years; fee for recertification application and evaluation is \$125 for members of the Society, and \$225 for non-members. Those that do not recertify, will be transferred into either an "Inactive" or "Retired" status.

If you were certified between January 1, 1975 and January 1, 1987, (anyone with a certificate number **lower than 725**), you must comply with this notice.

Each affected Certified Photogrammetrist has been sent a letter by Certified Mail, with the new forms and procedures. If you are reading this notice and have **NOT** received a letter, please call me immediately at 301-493-0290.

William D. French, CAE
Secretary, ASPRS